Commentary: JWST near-infrared detector degradation—finding the problem, fixing the problem, and moving forward

Bernard J. Rauscher[a]
NIRSpec Detector Scientist, Observational Cosmology Laboratory, NASA Goddard Space Flight Center, Greenbelt, MD, 20771, USA

Carl Stahle
NASA Detector Degradation Failure Review Board Chair, Instrument Systems and Technology Division, NASA Goddard Space Flight Center, Greenbelt, MD, 20771, USA

Robert J. Hill
NASA Detector Degradation Failure Review Board Assistant Chair, Observational Cosmology Laboratory, NASA Goddard Space Flight Center, Greenbelt, MD, 20771, USA[b]

Matthew Greenhouse
Integrated Science Instruments Module Project Scientist, Observational Cosmology Laboratory, NASA Goddard Space Flight Center, Greenbelt, MD, 20771, USA

James Beletic
Teledyne Imaging Sensors, 5212 Verdugo Way, Camarillo, CA, 93012, USA

Sachidananda Babu
Detector Systems Branch, NASA Goddard Space Flight Center, Greenbelt, MD, 20771, USA

Peter Blake
Optics Branch, NASA Goddard Space Flight Center, Greenbelt, MD, 20771, USA

Keith Cleveland
Mission Assurance Branch, NASA Goddard Space Flight Center, Greenbelt, MD, 20771, USA

Emmanuel Cofie
Mechanical Systems Analysis & Simulations Branch, NASA Goddard Space Flight Center, Greenbelt, MD, 20771, USA

Bente Eegholm
Optics Branch, NASA Goddard Space Flight Center, Greenbelt, MD, 20771, USA[c]

C.W. Engelbracht
Steward Observatory, University of Arizona, Tucson, AZ, 85721, USA

Donald N.B. Hall
Institute for Astronomy, University of Hawaii, Hilo, HI, 96720, USA

Alan Hoffman
Acumen Scientific, Goleta, CA, 93117, USA

Basil Jeffers
Parts Engineering Branch, NASA Goddard Space Flight Center, Greenbelt, MD, 20771, USA[d]

Christine Jhabvala
Detector Systems Branch, NASA Goddard Space Flight Center, Greenbelt, MD, 20771, USA

Randy A. Kimble
Integration & Test Project Scientist, Exoplanets and Stellar Astrophysics Laboratory, NASA Goddard Space Flight Center, Greenbelt, MD, 20771, USA

Stanley Kohn
Aerospace Corporation, El Segundo, CA, 90245, USA

Robert Kopp
Teledyne Imaging Sensors, 5212 Verdugo Way, Camarillo, CA, 93012, USA

Don Lee
Teledyne Imaging Sensors, 5212 Verdugo Way, Camarillo, CA, 93012, USA

Henning Leidecker
Electrical Engineering Division, NASA Goddard Space Flight Center, Greenbelt, MD, 20771, USA

Don Lindler
Exoplanets and Stellar Astrophysics Laboratory, NASA Goddard Space Flight Center, Greenbelt, MD, 20771, USA[c]

Robert E. McMurray Jr.

Instrument Technology Branch, NASA Ames Research Center, Moffett Field, CA, 94035,
USA

Karl Misselt
Steward Observatory, University of Arizona, Tucson, AZ, 85721, USA

D. Brent Mott
Detector Systems Branch, NASA Goddard Space Flight Center, Greenbelt, MD, 20771,
USA

Raymond Ohl
Optics Branch, NASA Goddard Space Flight Center, Greenbelt, MD, 20771,
USA

Judith L. Pipher
FGS Detector Scientist, Dept. of Physics & Astronomy, University of Rochester, Rochester, NY, 14627,
USA

Eric Piquette
Teledyne Imaging Sensors, 5212 Verdugo Way, Camarillo, CA, 93012, USA

Dan Polis
Materials Engineering Branch, NASA Goddard Space Flight Center, Greenbelt, MD, 20771,
USA

Jim Pontius
Mechanical Systems Analysis & Simulations Branch, NASA Goddard Space Flight Center, Greenbelt, MD, 20771,
USA

Marcia Rieke
NIRCam Principal Investigator, Steward Observatory, University of Arizona, Tucson, AZ, 85721,
USA

Roger Smith
California Institute of Technology, Pasadena, CA, 91125, USA

W.E. Tennant
Teledyne Imaging Sensors, 5212 Verdugo Way, Camarillo, CA, 93012, USA

Liqin Wang
Materials Engineering Branch, NASA Goddard Space Flight Center, Greenbelt, MD, 20771,
USA[e)]

Yiting Wen
Detector Systems Branch, NASA Goddard Space Flight Center, Greenbelt, MD, 20771,
USA

Christopher N.A. Willmer
Steward Observatory, University of Arizona, Tucson, AZ, 85721, USA

Majid Zandian
Teledyne Imaging Sensors, 5212 Verdugo Way, Camarillo, CA, 93012, USA

(Dated: 21 June 2012)

The James Webb Space Telescope (JWST) is the successor to the Hubble Space Telescope. JWST will be an infrared-optimized telescope, with an approximately 6.5 m diameter primary mirror, that is located at the Sun-Earth L2 Lagrange point. Three of JWST's four science instruments use Teledyne HgCdTe HAWAII-2RG (H2RG) near infrared detector arrays. During 2010, the JWST Project noticed that a few of its 5 μm cutoff H2RG detectors were degrading during room temperature storage, and NASA chartered a "Detector Degradation Failure Review Board" (DD-FRB) to investigate. The DD-FRB determined that the root cause was a design flaw that allowed indium to interdiffuse with the gold contacts and migrate into the HgCdTe detector layer. Fortunately, Teledyne already had an improved design that eliminated this degradation mechanism. During early 2012, the improved H2RG design was qualified for flight and JWST began making additional H2RGs. In this article, we present the two public DD-FRB "Executive Summaries" that: (1) determined the root cause of the detector degradation and (2) defined tests to determine whether the existing detectors are qualified for flight. We supplement these with a brief introduction to H2RG detector arrays, some recent measurements showing that the performance of the improved design meets JWST requirements, and a discussion of how the JWST Project is using cryogenic storage to retard the degradation rate of the existing flight spare H2RGs.

[a)] Bernard.J.Rauscher@nasa.gov

[b)] Also at Conceptual Analytics, LLC, Glenn Dale, MD, USA

I. INTRODUCTION

The James Webb Space Telescope (JWST) will be a 6.5 m class infrared optimized telescope located at the Sun-Earth L2 Lagrange point. As the successor to the Hubble Space Telescope, it is designed to enable a broad science program that includes studies of the first sub-galaxy sized clumps of stars to light up after the Big Bang, galaxy formation and evolution, the birth of stars and planetary systems, and the search for planets that can support life. It is infrared optimized because the cosmological expansion shifts the spectroscopic features that Hubble sees at visible wavelengths in the nearby universe into the infrared. Infrared wavelengths are also able to penetrate the heavily dust obscured regions of the universe where stars and planets form.

To enable this broad science program, JWST carries a suite of four science instruments: (1) a Near Infrared Camera (NIRCam), (2) a Near Infrared Spectrograph (NIRSpec), (3) a Fine Guidance Sensor (FGS) with Near-Infrared Imager and Slitless Spectrograph (NIRISS), and (4) a Mid-Infrared Instrument (MIRI). The three "near-infrared" (NIR; $0.6 \leq \lambda \leq 5$ μm) instruments use the Teledyne HgCdTe HAWAII-2RG (H2RG[1]) detector arrays that are the focus of this paper. The cutoff wavelength of an HgCdTe detector is tunable by varying the mole fraction of cadmium in the HgCdTe. The NIRSpec and FGS/NIRISS use 5 μm cutoff H2RGs, whereas NIRCam uses 2.5 μm and 5 μm cutoff H2RGs. The MIRI uses a different detector technology for the $5 - 29$ μm wavelength range, Raytheon Si:As blocked impurity band detectors. There has been no indication of any degradation in MIRI's detectors. We refer the interested reader to Gardner[2] and Greenhouse et al.[3] for more information about the JWST mission and its science instruments.

During April, 2010, the NIRSpec team noticed degradation of pixel operability in one 5 μm cutoff H2RG that had been stored for about 18 months at room temperature. By the end of the year, the NIRCam team had noticed similar changes in four more 5 μm cutoff H2RGs that had been stored for about two years at room temperature. One sign of degradation in JWST's H2RGs was an increase in the number of inoperable "warm pixels" (Fig. 1). JWST defines a warm pixel as a pixel having dark count rate $0.1 < $ rate $ < 60$ e^- s^{-1}, where the count rate is measured using a linear 2-parameter fit to the up-the-ramp samples spanning 1000 sec.

Warm pixels are most easily seen in dark images. A dark image is one for which the detector is enclosed in a completely blanked off dewar and continually reset until all memory of the previous warm or illuminated condition is erased. Although dark images should be very stable at constant temperature, changes are easily seen in degrading detectors like those shown in Fig. 1.

Soon after it was realized that the 5 μm detectors were degrading, NASA initiated a "Detector Degradation Failure Review Board" (DD-FRB) to address the following items.

(a) Determine the root cause of the detector degradation

(b) Determine manufacturing and/or post-manufacture handling/process changes to avoid it

(c) Define tests that are needed to screen-out degradation prone parts and ensure the continued integrity of flight parts

(d) Define tests to determine whether the existing detectors are qualified for flight

Within a few short months, the DD-FRB had determined root cause, identified design changes to eliminate the degradation, and also mitigations in case the existing detectors had to be flown. The DD-FRB wrote four Executive Summaries and a Final Report for items a-d. This article provides details for (a) and (d), while the information for (b) and (c) contains technical information that is proprietary to Teledyne Imaging Sensors as well as export controlled and International Traffic in Arms Regulations (ITAR) restricted. The ITAR is a set of United States government regulations that pertain to specified defense-related technologies including JWST's detector systems. Under ITAR, we cannot legally publish information that would facilitate duplicating the H2RG technology.

As is described in detail in Sec. II, the DD-FRB assigned root cause to a design flaw in the pixel's barrier layer that allows indium from the interconnects to inter-diffuse with gold in the contact structure and migrate into the HgCdTe detector material. Based on destructive physical analysis (DPA) of hybridized detectors and process evaluation chips (PEC[4]) from every flight detector, the DD-FRB concluded that "there is the potential for degradation in every pixel." The DPA of PECs is described in more detail in Sec. III.

Although it was clear that the performance of the 5 μm parts degraded more rapidly than the 2.5 μm parts, the DPA of PECs made it equally clear that the underlying physical process was active in both. Within the DD-FRB, this was referred to as a "dead pixel walking" scenario, the implication being that the performance of the 2.5 μm parts would eventually degrade if exposed to room temperature for a sufficient period of time. Moreover, because of the large number of variables that modulate the degradation rate, it was not possible to project the degradation rate for individual parts without performing

c) Also at Sigma Space Corporation, 4600 Forbes Blvd., Lanham, MD, 20706, USA

d) Also at MEI Technologies, Inc.
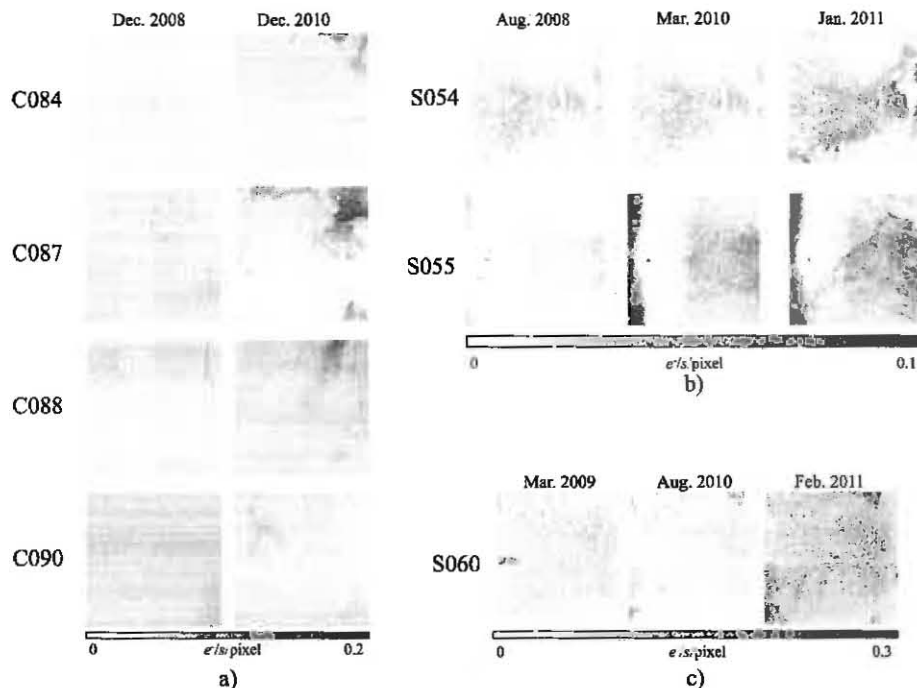
e) Also at Ball Aerospace, Boulder, CO, 80301, USA

FIG. 1. These dark images show the degradation versus time of several JWST 5 μm cutoff H2RGs. Each panel shows a dark image in inverse grayscale, where pixels with high currents show up as black. A dark image is a map of integrated charge under dark conditions. Parts prefixed with a "C" are NIRCam 5 μm H2RGs and parts prefixed with an "S" are NIRSpec 5 μm H2RGs. Panel a) shows degradation in four NIRCam parts, b) shows degradation in the NIRSpec "flight" parts, and c) shows the degradation of a NIRSpec "flight spare". Each dark image is taken with the detector enclosed in a completely blanked off dewar. The degradation manifests itself in the appearance of greater numbers of inoperable "warm" pixels.

destructive testing on a larger number of detectors than was available (see Sec. III).

For many applications, a reasonable work-around would be to keep the detectors cold as the indium inter-diffusion degradation process scales exponentially with temperature. Assembly of the JWST necessitates that the detectors withstand several years of room temperature storage prior to launch in 2018. For JWST, the plan is therefore to make additional flight detectors using an improved barrier layer design. To ensure maximum flexibility, the JWST Project is storing the existing flight spare detectors, which use the old barrier layer design, at cryogenic temperature to slow the degradation as much as possible. The rationale for this is given in Sec III.

This article is structured as follows. In Sec. I A, we provide a brief introduction to JWST H2RG detector arrays. Readers who are familiar with this technology and its application to JWST may wish to skip over this background material and go directly to Sec. II. The actual DD-FRB Executive Summaries comprise the bulk of the article in Secs. II and III. These are presented in as close to their original form as is practical in this journal. Because the two public Executive Summaries did not describe the specific design improvements that were made to eliminate degradation, we provide a high

level overview in Sec IV. In this section, we also discuss how the new design was validated for JWST. Finally, in Sec. V, we discuss some of the lessons learned and how the JWST project is storing its existing flight spare detectors under cryogenic conditions to slow the degradation as much as possible.

A. Brief Introduction to JWST H2RG Detector Arrays

1. H2RG Detector Arrays

The H2RG[5,6] (Fig. 2) is a hybrid NIR detector array. Light is collected in a 2040×2040 pixel array of HgCdTe photovoltaic diodes. The 2040×2040 pixel photosensitive area is surrounded on all sides by a 4 pixel wide border of reference pixels. For JWST, the entire 2048×2048 pixel area (reference pixels plus regular pixels) is read out using four analog outputs. The reference pixels, which have been engineered to electronically mimic a regular pixel, can be used to suppress correlated noise.[7,8] Electronic readout and control are accomplished in a silicon readout integrated circuit (ROIC). When it was first introduced,[6] HAWAII-2RG name refered only to the ROIC, although it is now common usage in the as-

tronomical community to refer to entire detector arrays as HAWAII-2RGs or H2RGs. The ROIC is permanently attached to the HgCdTe detector array by indium bump bonds. There is one indium bond per pixel. In the case of a JWST H2RG, a low viscosity epoxy is backfilled into the bumps to increase mechanical strength.

Unfortunately, the indium that is used to make the bump bonds does not interact well with some of the other materials that are used in the H2RG for their electrical or optical properties. As is described in Sec. II, indium interacts readily with gold in the contact structures to form In-Au intermetallic compounds.[9,10] Indium is an n-type dopant in HgCdTe, and in the JWST H2RG architecture, it is in close proximity to a p+ doped implant. Sec. II includes an extensive discussion of how indium penetrated the barrier layer in the H2RG design to interact with both gold and p+ doped HgCdTe to degrade the detectors.

2. JWST NIR Performance Requirements

Compared to many other applications, JWST places a premium on ultra low dark current and low read noise. JWST's H2RGs are read out at a 100 kHz pixel rate and biased to provide a well depth of about 10^5 e^-. JWST's NIR detector requirements derive principally from the need to observe extremely faint astronomical sources. In practice, this means that the quantum efficiency is required to be as good as is practical and the dark current noise is required to be low compared to noise resulting from the background Zodiacal flux. Tab. I lists an illustrative subset of the requirements that were flowed down from JWST's science program for NIRSpec. In practice, these NIRSpec requirements are slightly more challenging than what is needed for NIRCam and the Fine Guidance Sensor (FGS), but they give a good high level impression of the performance that is needed.

TABLE I. Selected JWST NIRSpec Detector Requirements

Parameter	Requirement
Operating temperature	$\sim 40 \ K$
Pixel pitch	18 μm
Pixel format	2040×2040 pixels
Pixel rate	100 kHz per output
# of outputs	4
Dark current	$i_{dark} < 0.01 \ e^- \ s^{-1} \ \text{pixel}^{-1}$
Total noise per 10^3 s	$< 6 \ e^- \ \text{rms}$
Read noise per CDS[a]	$< 21 \ e^- \ \text{rms}$
Quantum efficiency	$> 70\%$ for $0.6 - 1 \ \mu$m
	$> 80\%$ for $1 - 5 \ \mu$m

[a] The read noise per correlated double sample (CDS) is a derived requirement that is needed to enable the total noise requirement.

For most science observations, JWST will use an up-the-ramp readout scheme. Although each JWST instrument differs somewhat in the details, the basic idea is to destructively reset the detector array and then sequentially read it out to build up an integration one frame at a time. When the 2048×2048 pixel detector array is read out using four outputs at 100 kHz, the frame time is 10.73 s. This includes 12 pixels of overhead at the end of each row and one row of overhead at the end of each frame. Across JWST, approximately 10^3 s long integrations are taken as the baseline. For NIRSpec, this readout pattern produces one sample every 10.73 s and the baseline science integration contains 88 samples. The integrations are called up-the-ramp because when pixels are illuminated, the 88 up-the-ramp samples follow an approximately straight line with positive slope. For more information on JWST detector readout modes and noise models, the interested reader is referred to Rauscher et al.[11]

II. DD-FRB EXECUTIVE SUMMARY 2A: ROOT CAUSE DETERMINATION

This section presents DD-FRB Executive Summary 2a, the root cause finding. It is presented in as close to original form as possible, with only minor formatting and stylistic changes. Although we have tried to minimize duplication, some redundancy was unavoidable because each Executive Summary was intended as a stand alone document. The original document (JWST-RPT-017457; dated 29 April 2011) is available from the JWST public web site.[12]

A. Context and Statement of the Problem

The James Webb Space Telescope (JWST) science instrument payload contains four science instruments and a fine guidance sensor. Three of the science instruments and the fine guidance sensor utilize HgCdTe detectors that are designed to achieve high responsivity to light over the 0.6-5 μm spectrum. One instrument also utilizes HgCdTe detectors that are designed for the 0.6-2.5 μm spectrum. Seven of the 5 μm cut-off detectors and 8 of the 2.5 μm cutoff detectors are required for flight as shown in Tab. II.

Flight model integration has begun on all of the instruments listed in Tab. II. Teledyne Imaging Sensors produced all of the JWST HgCdTe detectors during the 2007-8 timeframe. The JWST assembly and test sequence requires that the science instrument detectors have an ambient temperature shelf life of several years prior to launch and an operational life of at least 5.5 years after launch.

Instrument team test data obtained over the past year has revealed degradation of pixel operability impacting several of the 5 and 2.5 μm cut-off detectors. There is
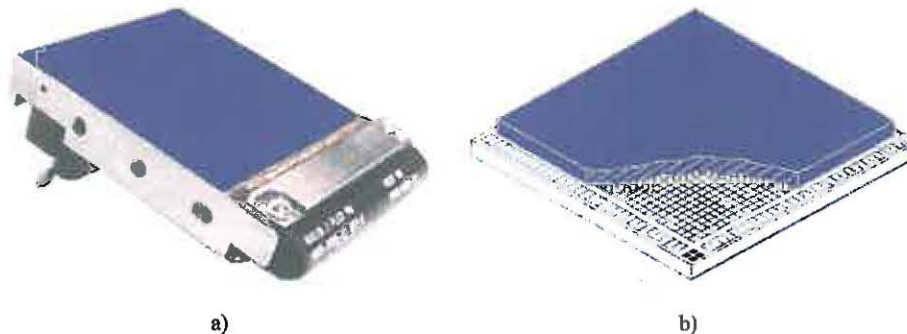
a)   b)

FIG. 2. a) This figure shows a NIRSpec H2RG detector array. The H2RGs used by NIRCam and FGS/NIRISS differ only in the mechanical packaging. The photosensitive area measures about 36.72×36.72 mm^2. The H2RG has 2040×2040 photosensitive HgCdTe pixels that are surrounded on all sides by a four pixel wide border of "reference pixels." b) Indium bump bonds are used to join the HgCdTe detector array to the silicon readout integrated circuit (ROIC).

TABLE II. HgCdTe sensors in the JWST ISIM

| Instrument | Agency | Quantity | |
		5 μm cutoff	2.5 μm cutoff
NIRCam	NASA	2	8
NIRSpec	ESA	2	N/A
FGS-TF[a]	CSA	1	N/A
FGS-Guider	CSA	2	N/A

[a] In the time since the DD-FRB completed its work, the FGS-TF was replaced with the Near-Infrared Imager and Slitless Spectrograph (NIRISS). The NIRISS uses the same detectors that were intended for the FGS-TF. To maintain consistency with the earlier DD-FRB reports, we retain the previous FGS-TF name here.
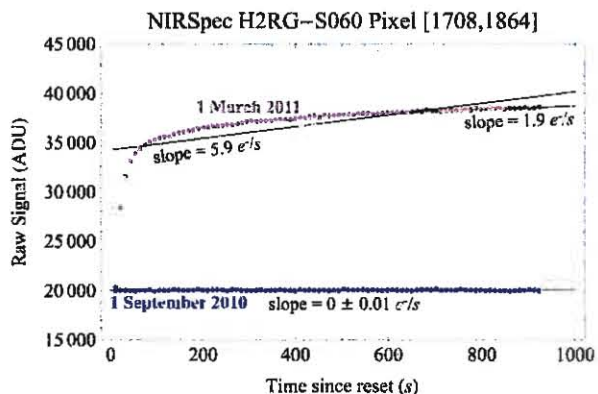

FIG. 3. Example of the increase in dark count rate for one pixel of a degraded detector. Here raw signal is measured in analog to digital converter units (ADU), and dark count rate is equal to the fitted slope. The blue data are for a good pixel and the red data are for the same pixel that has degraded with time.

a strong concern that the degradation will continue with time and many of the flight arrays will be out of specification by the time of launch. The key detector degradation observed was an order of magnitude increase in the dark count rate of individual pixels to levels in the range of 0.1 to 60 electrons per pixel per second (e^-/pix/sec). Fig. 3 shows an example of this increase in dark count rate for one pixel in a flight spare NIRSpec detector (S060). Other performance anomalies were also observed and are listed in Tab. III.

B. Root Cause Determination

The DD-FRB finds that the detector degradation is caused by a **design flaw in the barrier layer** of the pixel interconnect structure. The flawed barrier layer design makes the detectors vulnerable to migration of indium from the indium bump interconnect into the detector structure, degrading its performance.

The most obvious effect is the formation of an indium (In) gold (Au) intermetallic that is highly visible in Scanning Electron Microscopy (SEM) images taken during destructive physical analysis. The electrical data of degraded pixels reveal curved, "RC" shaped dark ramps that are indicative of parasitic capacitance, reactance, and shunting in the HgCdTe side of the interconnect. Typically a few hundred seconds after reset, true leakage currents become dominant. These effects cause pixels to fail to meet operability requirements.

Fig. 4a shows a cross-section of the pixel contact structure design. In this sensor design, each HgCdTe pixel is connected via the In bump to a source-follower amplifier in a silicon Read-Out Integrated Circuit (ROIC). The critically important barrier layer is intended to prevent In bump material from reacting with the Au pad and Au contact material such that it can not diffuse into the HgCdTe detector material. Figs. 4b and 4c show cross-sectional micrographs obtained with SEM of a non-degraded pixel from a 2.5 μm NIRCam detector array

(C105) and a degraded pixel from a 5 μm NIRCam detector array (C094). The cross-section of the pixel structure was generated by destructive physical analysis (DPA) using a focused ion beam (FIB) to cut through a line of pixels in the array. Fig. 4c shows the formation of an AuIn$_2$ intermetallic as well as a crack in the left corner of the pixel contact structure propagating into the HgCdTe detector. The intermetallic expands upon formation and most likely created a pocket of stress in the pixel.

Fig. 5a shows a diagram depicting failure of the barrier layer. Poor sidewall coverage of the layers over the step of the passivation layer or porosity of the barrier layer can allow In to inter-diffuse with the Au contact and Au pad metals to create In-Au intermetallics. Fig. 5b illustrates some potential degradation mechanisms; the intermetallic expansion may cause strain and lattice dislocation damage to the HgCdTe and/or enable In to diffuse into the p$^+$ HgCdTe of the implanted junction layer. Apart from production of charge traps in the semiconductor band gap, dislocation damage can also allow In or Au to diffuse more rapidly into the HgCdTe resulting in a dark current performance degradation rate that can be non-linear and difficult to reliably estimate.

Fig. 6 shows the flow diagram of the degradation mechanisms.

A degraded detector pixel can be modeled by an electrical circuit (Fig. 7), which produces an integration ramp signal with an "RC"-like curvature early in the ramp (see Fig. 3). More extensive damage or indium diffusion will produce additional leakage currents through the photodiode. Although this circuit model approximately captures the essential behavior of degraded pixels (an "RC" at early times and leakage at later times), the actual circuit elements are far from ideal.

Formation of the In-Au intermetallic was confirmed by Energy Dispersive x-ray Spectroscopy (EDS) to provide a direct measure of the elemental composition. Fig. 8a shows a SEM image of a corner of another detector pixel in detector array C094 with a corresponding elemental map for Au, In, and the barrier layer in Fig. 8b. For these samples, the cross-section was prepared by cutting through the sample with a wire saw followed by mechanical polishing. The data show the formation of the In-Au intermetallic with a break in the barrier layer at the sidewall of the contact opening.

Additional EDS data were taken on another pixel in detector C094 as well as the Process Evaluation Chip (PEC) for C094. Fig. 9a shows the SEM and the x-ray analysis area (red box) from the PEC and Fig. 9b shows the x-ray spectrum. Quantitative analysis of the weight percentage of the volume measured shows that the In-Au compound is AuIn$_2$.

Fig. 10 shows a SEM image and a backscatter electron image of a cross-section of a pixel in detector array C094. Combined with EDS analysis on the different regions, the results show that there is interdiffusion of both In and Au past the barrier layer with the formation of AuIn2 and AuIn intermetallics that expand in volume.

C. Key Physical Observations that Support Root Cause

To avoid focusing on a single aspect of the observed degradation, the DD-FRB developed a list of key observations that any root cause analysis would have to explain. This list began at 14 items and has since grown to 25 items, with each new observation adding or reinforcing the list (Tab. III). There are some common elements for all explanations: 1) formation for an RC circuit element, most likely an n/p or Schottky barrier that completely intercepts the circuit after the contact; and 2) defects which increase the detector junction leakage current. These common elements are likely caused by damage (dislocations, displaced ions) induced by the intermetallic formation itself due to an inadequate barrier layer. The damage is further increased in its effect by enhanced diffusion of indium, now present at or in the HgCdTe from the proximate In-Au intermetallic. Beyond this, every diode will have its own story, and there are millions of them in a detector array.

III. DD-FRB EXECUTIVE SUMMARY 2D: DEFINE TESTS TO DETERMINE WHETHER THE EXISTING DETECTORS ARE QUALIFIED FOR FLIGHT

This section presents DD-FRB Executive Summary 2d that defines tests to determine whether the existing detectors are qualified for flight. It is presented in as close to original form as possible, with only minor formatting and changes. The original document, which documents the situation as of July 2011, is available from the JWST public web site.[13]

A. Introduction

The DDFRB has released its findings for the root cause determination of the degradation of pixel operability impacting several of the 2.5 and 5 μm cutoff detectors used in the NIRCam, NIRSpec, and FGS instruments of the James Webb Space Telescope (JWST-RPT-017457, http://jwst.nasa.gov/resources/017457.pdf). The key finding is that the detector degradation is caused by a design flaw in the barrier layer of the pixel interconnect structure. The flawed barrier layer design makes the detectors vulnerable to migration of indium from the indium bump interconnect into the detector structure, degrading the performance of the detector. The fraction of pixels that are out of specification due to degradation over three years since manufacture ranges from 0.2% on some 2.5 μm arrays to 1-2% for the affected 5 μm arrays. Although these detector arrays as a whole are not yet out of specification, there is a strong concern that the degradation will continue with time and that many of the flight arrays will be out of specification by the time of launch. Likewise, there is a concern that there may be a latency period for the onset of measurable degradation once the

FIG. 4. a) Pixel contact structure; b) Scanning Electron Microscope (SEM) image of a non-degraded pixel in NIRCam detector C105; c) SEM of degraded pixel in NIRCam detector C094
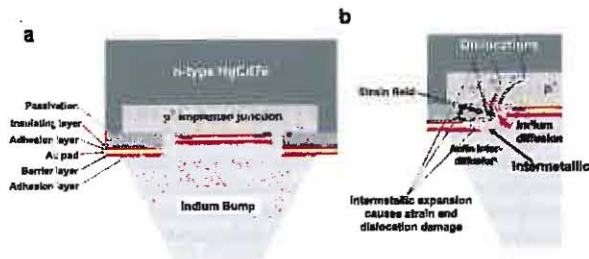

FIG. 5. (a) Inadequate barrier layer coverage; (b) Potential degradation mechanisms

barrier layer fails. Consequently, some of the detectors that currently show no sign of degradation may nevertheless degrade in the future. One of the tasks of the DD-FRB was to define tests to determine whether the existing detectors are qualified for flight. The DD-FRB identified two tests:

1. A Destructive Physical Analysis (DPA) test using Focused Ion Beam dissection in conjunction with Scanning Electron Microscopy (FIB/SEM) on Process Evaluation Chips (PECs) for each flight detector to determine the presence of In-Au intermetallics in the pixel structure.

2. Accelerated life testing with temperature bakes on the Sensor Chip Assembly (SCA) to determine the degradation rate.

The DPA tests on the PECs for each flight detector showed the presence of an In-Au intermetallic in every pixel examined. The key conclusion from these tests is that every pixel in every flight detector most likely has an In-Au intermetallic, so there is the potential for degradation in every pixel. This analysis could be used as a disqualification test. Based on the methodology presented in Executive Summary 2c, an accelerated life test could be applied to the existing SCAs to determine the degradation rate. It may be possible to bound the risk by performing destructive accelerated life testing on a few of the existing spare SCAs.

B. Destructive Physical Analysis on Process Evaluation Chips for Flight Detectors

The DD-FRB finds that every pixel in every flight detector most likely has an In-Au intermetallic so there is the potential for degradation in every pixel. This result is based on Destructive Physical Analysis (DPA) using a Focused Ion Beam (FIB) to cross-section an individual pixel and then Scanning Electron Microscopy (SEM) to image the pixel structure. FIB/SEM was done on 3 pixels in a 400 pixel mini-array from a Process Evaluation Chip (PEC) for every flight detector. A total of 72 pixels from 24 PECs were tested and every pixel showed the formation of In-Au intermetallics from the failure of the barrier layer. Fig. 11 shows the SEM images of individual pixels from a 2.5 μm detector (NIRCam) and 5 μm detectors (NIRCam, NIRSpec, and FGS).

C. Projecting Future Performance

Once the barrier layer fails, the subsequent degradation of a detector array is a complex and highly variable process. To understand the issues, it is helpful to focus on a single degrading pixel. If the future degradation of an individual pixel could be projected, the degradation of an entire SCA could be treated as the projection of an ensemble of pixels.

Detector degradation due to In diffusion is a multi-faceted process that begins when the barrier layer fails. The failed barrier layer allows In and Au to inter-diffuse, forming In-Au intermetallics. The formation of these intermetallics creates mechanical stress that may create dislocation defects deep into the pixel. Although In is a slow diffuser in HgCdTe, it is a fast diffuser along dislocation defects. Once the In reaches a sensitive area of the pixel, it creates a "warm pixel" (a pixel exhibiting an
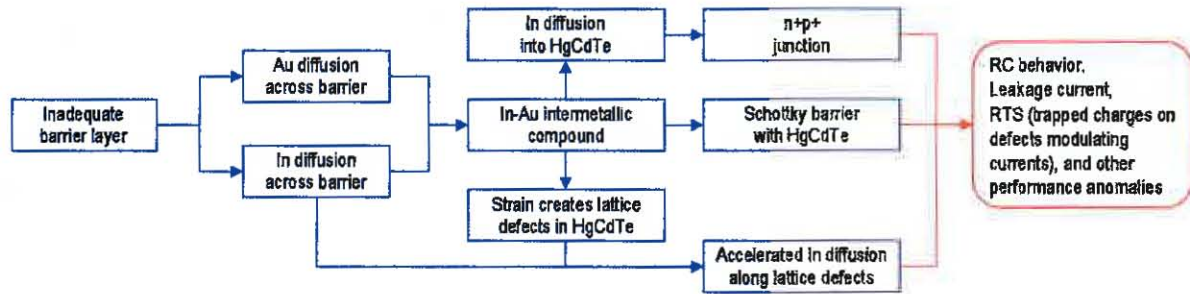
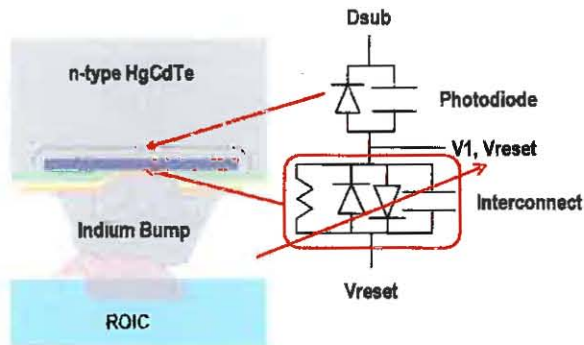FIG. 6. Degradation process in a pixel due to inadequate barrier layer

FIG. 7. This electrical circuit model of a degraded pixel accounts for the "RC"-like curvature of dark ramps (see Fig. 3). The red-highlighted components form in the HgCdTe immediately above the failed barrier layer. These cause the "RC"-like shape. This simple model does not attempt to explain the degradation in the photodiode that causes enhanced leakage current.
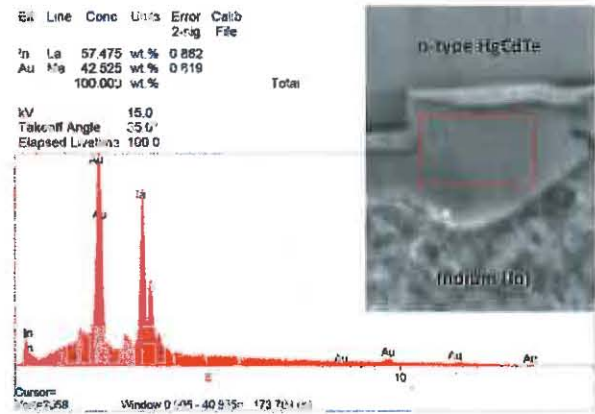

FIG. 9. a) X-ray analysis (EDS) of red box area in SEM image demonstrates the presence of an In-Au intermetallic ($AuIn_2$)
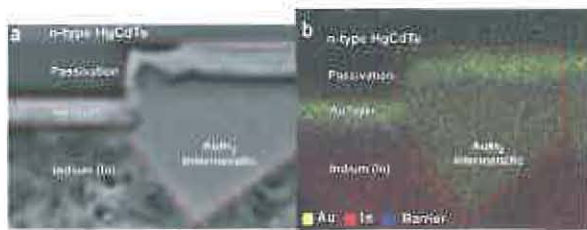

FIG. 8. a) SEM of a pixel corner in NIRCam detector C094; b) X-ray elemental analysis (EDS) of the same area showing that Au and In have interdiffused to form an intermetallic compound ($AuIn_2$) due to failure of the barrier layer
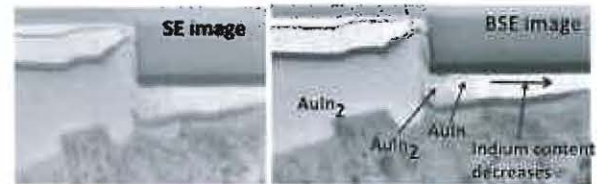

FIG. 10. SEM and Backscatter Secondary Electron (BSE) image of detector pixel in C094

increase in dark current) by the mechanisms discussed in Executive Summary 2a.

For purposes of this discussion, we make a simplifying assumption that the degree of degradation of a pixel is roughly proportional to the amount of In that has diffused in. The actual degradation process can be more complicated, but a simple scaling argument is sufficient to show the large number of unconstrained variables that must be included to model even one pixel. These variables include: (1) diffusion area, (2) diffusion permeability, (3) number of dislocation defects that intersect the diffusion area, (4) diffusion coefficient for each dislocation defect, (5) depth to the first sensitive area in the pixel, and (6) the scaling factor between In concentration and dark current. Moreover, the number of dislocation defects is likely to depend on (7) the number of thermal cycles, and (8) the diffusion coefficient is likely to be variable along a defect. By picking parameters in a Monte Carlo simulation, it is possible to obtain any degradation

TABLE III. Key Physical Observations

1	The number of warm pixels[a] increases with time in both the 2.5 μm and 5 μm cutoff detectors that show degradation.
2	"In degraded detectors[b], some warm pixels get better at the same time as a larger number get worse."
3	The rate of degradation of the detectors varies from part to part and is not necessarily linear with time.
4	"Although clustered, the new warm pixels do not form a contiguous group."
5	"The spatial distribution of the warm pixels appears to be similar for all the NIRCam 5 μm detectors. In addition, there are similarities in the spatial distribution of warm pixels among the affected NIRSpec detectors, but the distributions are different from those of the NIRCam parts. However, there is at least one small area near the edge of the detectors with a higher density of warm pixels that is common to both the NIRCam and NIRSpec parts."
6	"No warm pixels have been observed in the reference pixels of any degraded detector, even though new warm pixels are seen in the immediately adjacent regions of some degraded detectors."
7	Areas with an increased density of warm pixels also show a small decrease in flat field response relative to good regions.
8	"While some new warm pixels may be hot pixel[c] neighbors, most new warm pixels are not related to hot pixels."
9	The regions with high densities of new warm pixels are preferentially found near the edges of the detectors rather than at the centers. These regions are also where the stress-induced curvature of the detectors is at a minimum.
10	"A 12hr bake at 50C in a dry nitrogen environment resulted in an increased number of warm pixels, indicating an increased rate of formation while at elevated temperature in one of the degraded NIRCam 5 μm detectors (C094)."
11	"The new warm pixels that appeared after the 12hr-50C bake of C094 have a similar spatial distribution and electrical properties (dark count rates, ramp shapes) as the pixels that had become warm during ambient storage."
12	"The character of the degradation of some WFC3 detectors at their operating temperature of 145K is very similar to that of the JWST detectors at their 40K operating temperature, despite the differences in the long wavelength cut-off (1.7m vs. 5 μm), processing details, and subsequent storage and handling. It is possible that the same physical processes are at work in both instances, while the details may differ."
13	"Eight of the eleven tested 5 μm detectors show degradation. However, only two out of thirteen 2.5 μm detectors have degraded. In addition, two FGS 5 μm detectors show no degradation but have been stored in ambient conditions for 1 year less than the other JWST detectors."
14	The slope of the dark signal ramps for most (80-85%) new warm pixels shows statistically significant curvature (RC-like behavior).
15	"For a large fraction of the new warm pixels in NIRSpec detector S060 (5 μm), the dark count rate is approximately independent of temperature at low temperatures (T < 80K). However, at higher temperatures (80-100K), a dependence of the dark count rate on temperature is observed, indicating that a different mechanism is dominant in each of the two temperature regimes."
16	A change in temperature from 37.5K to 41K can result in some apparently good pixels becoming bad for S060.
17	"Under the assumption of normal gain, the noise in some, or all, new warm pixels, while higher than for good pixels, is lower than expected from shot noise associated with the measured signal."
18	"For S060, the asymptotic value of the dark count rate is consistent with the noise enhancement in degraded pixels. For this detector, the degradation manifests as a) the appearance of an RC behavior shortly after reset, and b) real leakage current that dominates the RC after a few hundred seconds."
19	The two 2.5 μm detectors (C038 & C041) that have exhibited an increase in warm pixels show an even larger fraction of warm pixels (relative to the mean) when measured at higher temperatures (90K for C038 and 85K for C041).
20	The region of C038 that exhibits an increased density of warm pixels (at both 39.5K and 90K) also shows a decrease in well depth.
21	Most of the warm pixels in C041 become good when the detector is cooled to 23.4K.
22	Multiple labs have observed the same phenomena in different test sets.
23	The Scanning Electron Microscope (SEM) and Energy Dispersive x-ray Spectroscopy (EDS) analysis of C094 shows that an In-Au intermetallic has formed in all 15 pixels examined to date. These include examples of both degraded and non-degraded pixels. SEM analysis of the Process Evaluation Chip (PEC) associated with this detector also shows the In-Au intermetallic in all pixels examined. The major intermetallic formed is $AuIn_2$. $AuIn$ is also formed next to the $AuIn_2$ where there was originally Au.
24	SEM analysis of the PEC associated with the good (i.e. showing no degradation) 2.5 μm detector C105 shows no indication of In-Au intermetallic formation.
25	"SEM analysis of the PEC associated with the 5 μm detector S042 shows that an In-Au intermetallic has formed, although the intermetallic volume appears to be less than in C094. This detector has shown no degradation as of the most recent testing in Jan. 2010."

[a] **Warm (degraded) pixel:** A pixel with a dark count rate $0.1 < rate < 60 \ e^- \ s^{-1}$, where the count rate is measured using a linear 2-parameter fit to the up-the-ramp samples spanning 1000 sec.

[b] **Degraded detector:** A detector that exhibits a statistically significant increase in the number of warm pixels.

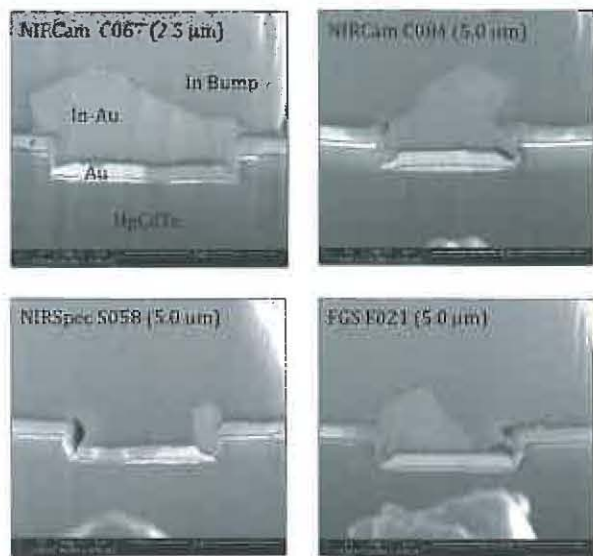[c] **Hot pixel:** A pixel having higher leakage current than a warm pixel.

FIG. 11. Scanning Electron Microscopy images of pixels from a Process Evaluation Chip of NIRCam, NIRSpec, and FGS flight detectors. The presence of In-Au intermetallics from the breakdown of the barrier layer, as indicated by lighter shading in the In and Au layers, is present in all of the images.

path from no degradation to all pixels simultaneously going out of specification. However, it does not follow that all such possible distributions arise in reality.

The only way out of this conundrum is to make on the order of tens of measurements to constrain these unknowns, with clear degradation between each measurement. In addition, it would also be necessary to degrade the SCA to at least the onset of rapid degradation to constrain some of the most important parameters. The DD-FRB believes that a research program like this is not practical for the current JWST flight detectors due to a very limited inventory of SCA samples that are available. In order to not get fooled by small number statistics, we estimate that a minimum of 10 SCAs of both 2.5 and 5 μm cut-off wavelength are needed for these measurements. We have currently identified 5 candidate SCAs at each wavelength.

D. Bounding the Risk

The DD-FRB realizes that a full complement of better SCAs may not be available for JWST when they are needed. For this reason, the DD-FRB considered what steps the JWST Project might take to bound the risks associated with using the existing SCAs if necessary. Because detector degradation depends on so many factors, and these factors differ widely from one detector to the next, the main risks are associated with statistical outliers.

The most we can hope to do is to gain some information on the range of degradation paths (e.g. the shapes of the warm pixel percentage vs. time curves) that a pool of SCAs might experience in the future. Accelerated testing (through a combination of elevated temperature storage and thermal cycling) may, for example, may provide information about the prevalence of two potentially distinct degradation behaviors:

1) The pixel-destroying indium diffusion process has a critical step with a characteristic latency period, such that little degradation is seen for an extended time period, and that rapid degradation then ensues, yielding a highly non-linear, "degradation cliff" behavior to the long-term bad pixel trend for a SCA. This degradation path is the worrisome case, for the situation where that cliff occurs within the ground storage period of the detectors. One could have SCAs whose performance still looks perfectly acceptable at the last reasonable replacement opportunity, but which would nonetheless degrade unacceptably before launch.

2) There are intrinsically wide distributions in the values of the physical parameters (the assorted defects) that determine a pixel's future behavior. These wide distributions convolve to yield a wide range in the latency period before serious degradation of individual pixels occurs. In this case, the composite degradation of a large ensemble of pixels would be more gradual, and a SCA, as a whole, would not exhibit a performance "degradation cliff" that will put it out of specification by the time of launch.

The DD-FRB believes it would be useful to measure some information regarding the relative prevalence of these behaviors. However, we recognize that with only a small pool of devices available for accelerated life testing, such tests are quite limited with respect to their ability to make strong statements regarding the future behavior of current flight SCAs. If, in a small sample of devices, a significant number were shown to exhibit the cliff-like degradation behavior on an accelerated timescale that corresponds roughly to the required ground storage period, there would be reason for grave concern about even SCAs that still have acceptable performance. If, in contrast, all of the SCAs that are monitored or put through accelerated life testing show gradual, smooth degradation versus time throughout the relevant time period, then one could make a reasonable inference that parts with a smooth degradation projection will likely remain that way.

By subjecting a few of the existing SCAs to accelerated life testing, it should be possible to understand how the average SCA will evolve, and moreover to place some loose bounds on the likely dispersion around that average. For purposes of this testing, the 2.5 μm and 5 μm cutoff SCAs would need to be considered as separate populations. A JWST SCA could be baked at a maximum temperature of 50 C over an extended period of time to monitor degradation (50 C is the maximum temperature that occurs in the SCA fabrication process). Additional stresses, which will not be encountered in the flight application, may be introduced at higher temperatures. Once

this testing is done, there will still be a residual risk of statistical outliers in the existing detector complement, and the JWST Project would need to properly account for the risk that a few flight detectors might unexpectedly degrade more (possibly much more) than is projected even when the measured dispersion around the mean is taken into account to arrive at a worst case statistical projection. The JWST Project would have to evaluate the impact of this risk for each science instrument.

To lower the risk that a full complement of replacement detectors are available when needed to preserve the JWST mission schedule, the DD-FRB recommends storing the current flight spare SCAs at cryogenic temperature to retard their degradation rate. Although we don't know the exact functional dependence of the degradation rate, previous experience with HgCdTe detectors for diffusion and electrical activation processes suggests an exponential dependence on temperature so a SCA should be stored at the lowest practical temperature to greatly reduce the risk of further degradation.

E. Summary

The DD-FRB finds from destructive physical analysis tests on Process Evaluation Chips for each flight detector that every pixel in every flight detector most likely has an In-Au intermetallic so there is a high potential for degradation in every pixel – a "dead pixels walking" scenario. It may be possible to place bounds on the expected degradation with ambient temperature storage time by subjecting a few of the existing SCAs to accelerated life testing. The current flight spare SCAs should be stored at the lowest practical temperature to reduce the risk of degradation.

IV. IMPROVED JWST H2RG DESIGN & CRYOGENIC STORAGE

As has already been mentioned, JWST is in the process of making additional flight detector arrays using an improved design that eliminates the degradation's root cause. In Sec III, the DD-FRB recommended storing the existing flight spare H2RGs at cryogenic temperature to retard the degradation rate. We discuss these topics in the following paragraphs.

A. Improved Barrier Layers

The details of how the root cause of degradation was eliminated are ITAR sensitive Teledyne Proprietary information. As such, this discussion is very high level. Teledyne is working on an article that will explain the new design in more detail.[14]

Executive Summary 2a (Sec. II) pinpointed the root cause of the degradation as, "a design flaw in the barrier layer of the pixel interconnect structure." The corrective actions taken included: (1) redesigning the barrier layer (see Fig. 5) and (2) process improvements aimed at achieving more uniform and conformal barrier layer coverage.

The improved design uses different materials for the barrier layer. Component level laboratory testing at Goddard and Teledyne showed that the specific material that was used for the primary barrier in the JWST H2RG design was permeable to indium. The improved design uses a different combination of materials that the same testing shows are completely impermeable to indium, even at temperatures warmer than room temperature.

A second aspect of the improved design is applying the barrier layer in a more conformal way. SEM imagery, including Fig. 4, showed that the old barrier layer design did not achieve good step coverage. The improved barrier layer is applied using newer processes that achieve better step coverage. Also, some aspects of the interconnect structure were modified to facilitate achieving good step coverage.

B. Validating the New Design

Validating the new design requires: (1) tests showing that the degradation had been completely eliminated and (2) tests showing that the improved design meets JWST performance requirements. By March, 2012, sufficient progress had been made in both areas for JWST to resume flight production. All testing to date has been successful, with no indication of any problems associated with the new design.

1. Tests Showing that Degradation was Eliminated

In order to show that the new detector design is not susceptible to degradation, Teledyne built a demonstration lot of H1RG SCAs that incorporate the new barrier layer. An H1RG is a 1K×1K pixel SCA that uses the same pixel design as the H2RG. The DD-FRB recommended two kinds of accelerated life testing to demonstrate the validity of the improved barrier layer design. These were (1), showing through DPA that the new barrier layer remains intact after thermal cycling and a high temperature bake and (2) life testing of the new SCAs to show that no degradation occurs over the required JWST lifetime.

During the course of the DD-FRB, anecdotal evidence was acquired regarding the stability of the new design through the baking of several samples followed by DPA. The barrier layer remained intact in all cases. However, while encouraging, the results are not conclusive because the samples were not fully realized SCAs and hence were not subject to the same stresses (hybridization and thermal cycling) that the JWST detectors will encounter.

The high temperature bake test is a worst-case scenario that consists of taking two demonstration lot SCAs, subjecting them to 30 thermal cycles between room temperature and 35 K, a 100 C bake for 30 days, and another 20 thermal cycles prior to performing a DPA. The 30 day bake at 100 C provides the equivalent of a 10 year lifetime at room temperature for a thermal process with an activation energy of 0.58 eV. The formation of the In-Au intermetallic has higher activation energy (~0.68-0.72 eV)[9,10] and hence, the bake should provide sufficient margin against the room temperature storage time for future JWST detectors (as much as 7 years). The SCAs are currently undergoing the 30 day bake and the DPA results will be available in May 2012.

The JWST flight detectors will never be subjected to temperatures above 45 C, and therefore a completely valid life test must be conducted at this temperature or lower to insure that there is no significant degradation mechanism with an even lower activation energy than 0.58 eV. Unfortunately, this relatively low temperature limit means that the life test requires extended bake times to provide the equivalent of a 7 year room temperature storage lifetime. The bake tests will therefore run for 2.5 years, with performance tests interspersed at roughly 6 month intervals. For each of the 5 μm and 2.5 μm cut-off wavelength detectors, two SCAs will be baked at 45 C and two more will be baked at 35 C, while others will be stored at room temperature. If any degradation is observed, the rate of degradation seen at each temperature can be used to determine the activation energy of the degradation process. This test will not just be sensitive to the formation of the In-Au intermetallic, but will uncover any thermally activated degradation mechanisms with activation energies as low as ~0.35 eV. The initial performance testing of the SCAs to be baked in these tests are currently being completed.

2. Tests Showing that Performance Requirements are Met

Teledyne and the JWST Project validated the new barrier layer design's performance by testing prototype H1RGs at Teledyne, the University of Arizona, and in the Goddard Detector Characterization Laboratory (DCL). All three labs agree that the prototype H1RGs have performance comparable to the current flight parts when they were new and had little or no degradation. In the following paragraphs, we briefly summarize some of the test results for the first two flight-design 5 μm H1RG prototypes that were tested in the DCL. These tests showed that the parts either met flight specification, or exhibited only minor non-compliances that were completely consistent with the current flight parts that use the old design.

The DCL is responsible for NIRSpec detector characterization. It is equipped with an ultra-low background cryocooled dewar capable of operating the detectors at $T \approx 40$ K. This dewar routinely achieves dark currents

< 0.01 $e^- s^{-1}$ and read noise per correlated double sample (CDS), $\sigma_{CDS} < 12$ e^- rms when testing flight grade NIRSpec detectors. The NIRSpec dewar is equipped with an internal cryogenic integrating sphere and Judson InSb diodes for measuring absolute QE. For the measurements that are reported here, an external monochromator was used to provide $R = \lambda/\Delta\lambda \approx 100$ illumination. We refer the interested reader to Mott[15] for more information about the NIRSpec test setup in the DCL.

Tab. IV summarizes the performance of two new H1RG sensor chip assemblies (SCA) vs. NIRSpec requirements when operated at T=38 K. These are the first two of five prototype H1RGs that will be tested for NIRSpec this spring. For reference, we provide the average measurements for the NIRSpec flight (S54 & S55) and flight spare (S58 & S60) detectors that use the old barrier layer design. These are the best four detector arrays produced out of approximately 60 that were made during NIRSpec's initial production. If the two prototypes appear be be slightly lower performing in some area (e.g. dark current), it is important to recall that the current flight parts that serve as the basis for comparison were cherry picked from a much larger sample.

Fig. 12 shows that the measured responsive quantum efficiency (RQE) generally meets requirements to within the ±10% zero point uncertainty of the measurement. The improved barrier layer parts do not meet specification at every wavelength, but the same could be said for the old design parts. At the shortest wavelengths, the RQE is strongly modulated by the AR coating. The new barrier layers are buried deep in the detectors where only long wavelength photons can reach. There is no evidence that the improved barrier layer design has lower overall RQE performance than the old design.

Overall, testing at Teledyne, in the Goddard DCL, and at the University of Arizona has shown that the new barrier layer parts are very high performing, and certainly no worse than old design parts when the performance is looked at comprehensively. The NIRSpec team plans to present more test results for improved barrier layer NIRSpec parts when the prototype program finishes this summer. Teledyne plans to present more information on the improved barrier layer design and performance this summer.[14] The University of Arizona and Canadian Space Agency will provide more information on the performance of improved barrier layer parts for the NIRCam and FGS respectively as part of the normal work of building the instruments.

C. Cryogenic Storage of Existing Flight Spares

Executive Summary 2d did not specify cryogenic storage parameters, but colder is clearly better. JWST accepted the DD-FRB's cryogenic storage recommendation, and the flight spares that use the design that can degrade are being stored at the coldest practical tem-

TABLE IV. Measured Performance of Prototype H1RGs

Parameter	Unit	Requirement	SCA16684	SCA16686	Old Design
Dark current[a]	$e^-\ s^{-1}$	< 0.01	0.0099	0.0113	0.0053
Total noise[b]	e^-rms	< 6	5.75[c]	5.34[c]	6.48[d]
Crosstalk[e]	%	< 5%	1.2	1.5	1.2

[a] The dark current of the H1RG prototypes may be limited by the ROIC. More testing is planned using H2RGs for flight.

[b] Computed on a per pixel basis using at least 40 integrations. 88 non-destructive reads are allowed in each 10^3 s integration. See Rauscher[11] for more information on the baseline NIRSpec readout mode.

[c] Measured using a Gen-III Leach controller.

[d] Limited by SIDECAR ASICs when operated at T≈40 K with <20 mW of allowed power dissipation. See Moseley[7] and Rauscher[8] for a discussion of noise in SIDECAR based H2RG detector systems.

[e] Computed as the average crosstalk to each of the four nearest neighbors.
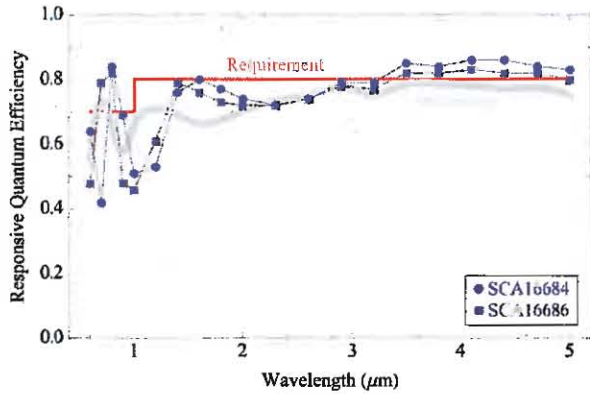

FIG. 12. The responsive quantum efficiency (RQE) of the new improved barrier layer detector arrays generally meets JWST requirements to within the ±10% zero point uncertainty for these measurements. This figure shows the RQE of two improved barrier layer H1RGs overlaid on NIRSpec requirements (Red) and the average of the four old-design NIRSpec "flight" and "flight spare" H2RGs (Gray). The H1RG prototypes use a NIRCam AR coating that is optimized for longer wavelengths than the NIRSpec coating that was used for the old design H2RGs. When this is taken into account, the performance of the improved barrier layer design is no worse than the old design.

peratures. These differ from one instrument to another based on what makes the most sense at the relevant lab.

NIRCam plans to store six flight spares at the University of Arizona. The two 2.5 μm cutoff H2RGs and four 5 μ cutoff H2RGs will be stored in a commercial freezer at T~-80 C. At the time of writing, the details of how NIRCam will store the parts are still being worked out.

For NIRSpec and FGS, five H2RGs will be stored in a dewar in the NASA Goddard Space Flight Center Detector Characterization Laboratory (DCL) at T~60 K. These are as follows;

- one complete NIRSpec flight spare focal plane array containing two 5 μm cutoff H2RGs,

- two individual NIRSpec 5 μm cutoff H2RGs, and

- one complete FGS flight spare focal plane array containing one H2RG.

V. CONCLUSION

In this article, we presented the JWST DD-FRB's two public Executive Summaries. The first explains the root cause for why some of JWST's 5 μm cutoff HgCdTe H2RGs degraded after 1.5-2 years of room temperature storage. The second explains why all of JWST's H2RGs built up through 2009 (both 5 μm and 2.5 μm cutoff) have the potential to degrade and recommends cryogenic storage to slow the degradation rate. As of March, 2012, JWST is making additional H2RGs that use an improved barrier layer design that eliminates the root cause of degradation. Furthermore, the JWST project accepted the DD-FRB's recommendation to store detectors at the coldest practical temperature. The NIRCam flight spares will be stored in a commercial freezer at T~-80 C. The NIRSpec spares and an FGS spare will be stored in a cryogenic dewar at T~60 K.

There are two important lessons learned from this investigation. One lesson is the need to use reliability engineering in the production of complex detector arrays such as HgCdTe detectors to predict the performance reliability for a given lifetime under specific operating and storage conditions. Accelerated life testing on test coupons such as the PECs and sample SCAs provides critical information for the reliability analysis as well as information on potential degradation mechanisms. If a degradation mechanism is identified and correlated to a physical property of the detector array, it is important to use manufacturing quality assurance procedures such as destructive physical analysis as a screening test to remove parts that have a higher probability of failure.

A second lesson that enabled the success of this investigation is the need to create a team of engineers and scientists from the appropriate government agencies, industry, and universities with diverse skills in the physics, fabrication, testing, materials science, reliability, and specific application of detector arrays to resolve subtle and complex detector degradation issues. This enabled the DD-

FRB to quickly find the problem, fix the problem, and recommend a path to move forward within the cost and schedule challenges of the JWST project.

ACKNOWLEDGMENTS

[1] Although the acronym H2RG refers only to the readout integrated circuit, here we follow convention in the astronomical community and use it to refer to the complete hybrid detector array.

[2] J. P. Gardner, J. C. Mather, M. Clampin, R. Doyon, M. A. Greenhouse, H. B. Hammel, J. B. Hutchings, P. Jakobsen, S. J. Lilly, K. S. Long, J. I. Lunine, M. J. McCaughrean, M. Mountain, J. Nella, G. H. Rieke, M. J. Rieke, H.-W. Rix, E. P. Smith, G. Sonneborn, M. Stiavelli, H. S. Stockman, R. A. Windhorst, and G. S. Wright, "The James Webb Space Telescope," Space Sci. Rev. **123**, 485–606 (Apr. 2006), arXiv:astro-ph/0606175.

[3] Matthew A Greenhouse, Vicki Balzano, Pamela Davila, Michael P Drury, Jamie L Dunn, Stuart D Glazer, Ed Greville, Gregory Henegar, Eric L Johnson, Ray Lundquist, John C Mccloskey, Raymond G Ohl, Robert A Rashford, and Mark F Voyton, "Status of the james webb space telescope integrated science instrument module system," UV/Optical/IR Space Telescopes and Instruments: Innovative Technologies and Concepts V. Edited by Tsakalakos **8146**, 262 (Sep 2011), http://adsabs.harvard.edu/cgi-bin/nph-data_query?bibcode=2011SPIE.8146E.262G&link_type=ABSTRACT.

[4] The processed detector wafers are evaluated by current-voltage and optical testing of PECs. PECs are lithographically patterned adjacent to the main array(s) on the wafers, and are diced and wirebonded into leadless chip carrier (LCC) packages for cryogenic testing. They contain variable sized photodiodes, small test arrays, contact measurement structures, and other test devices used for evaluating the diode performance (dark current, quantum efficiency, contact resistance) and materials properties (diffusion length, carrier lifetime, etc.) for each processed wafer.

[5] Markus Loose, James Beletic, James Garnett, and Min Xu, "High-performance focal plane arrays based on the hawaii-2rg/4g and the sidecar asic," Focal Plane Arrays for Space Telescopes III. Edited by Grycewicz **6690**, 10 (Sep 2007), http://adsabs.harvard.edu/cgi-bin/nph-data_query?bibcode=2007SPIE.6690E.10L&link_type=ABSTRACT.

[6] Markus Loose, Mark C Farris, James D Garnett, Donald N. B Hall, and Lester J Kozlowski, "Hawaii-2rg: a 2k x 2k cmos multiplexer for low and high background astronomy applications," IR Space Telescopes and Instruments. Edited by

John C. Mather Proceedings of the SPIE **4850**, 867 (Mar 2003), http://adsabs.harvard.edu/cgi-bin/nph-data_query?bibcode=2003SPIE.4850.867L&link_type=ABSTRACT.

[7] S. H Moseley, Richard G Arendt, D. J Fixsen, Don Lindler, Markus Loose, and Bernard J Rauscher, "Reducing the read noise of h2rg detector arrays: eliminating correlated noise with efficient use of reference signals," High Energy **7742**, 36 (Jul 2010), http://adsabs.harvard.edu/cgi-bin/nph-data_query?bibcode=2010SPIE.7742E.36M&link_type=ABSTRACT.

[8] Bernard J Rauscher, Richard G Arendt, D. J Fixen, Matthew Lander, Don Lindler, Markus Loose, S. H Moseley, Donna V Wilson, and Christos Xenophontos, "Reducing the read noise of hawaii-2rg based detector systems with improved reference sampling and subtraction (irs2)," Infrared Sensors **8155**, 45 (Sep 2011), http://adsabs.harvard.edu/cgi-bin/nph-data_query?bibcode=2011SPIE.8155E.45R&link_type=ABSTRACT.

[9] J. E Jellison, "Gold-indium intermetallic compounds: Properties and growth rates," NASA Document, 1–45(1979), http://misspiggy.gsfc.nasa.gov/tva/meldoc/photonicsdocs/Jane.pdf&link_type=EJOURNAL.

[10] G.W Powell and J.D Braun, "Diffusion in the gold-indium system," Trans. AIME **230**, 694–699 (Jun 1964).

[11] B. J. Rauscher, O. Fox, P. Ferruit, R. J. Hill, A. Waczynski, Y. Wen, W. Xia-Serafino, B. Mott, D. Alexander, C. K. Brambora, R. Derro, C. Engler, M. B. Garrison, T. Johnson, S. S. Manthripragada, J. M. Marsh, C. Marshall, R. J. Martineau, K. B. Shakoorzadeh, D. Wilson, W. D. Roher, M. Smith, C. Cabelli, J. Garnett, M. Loose, S. Wong-Anglin, M. Zandian, E. Cheng, T. Ellis, B. Howe, M. Jurado, G. Lee, J. Nieznanski, P. Wallis, J. York, M. W. Regan, D. N. B. Hall, K. W. Hodapp, T. Böker, G. De Marchi, P. Jakobsen, and P. Strada, "Detectors for the James Webb Space Telescope Near-Infrared Spectrograph. I. Readout Mode, Noise Model, and Calibration Considerations," PASP **119**, 768–786 (Jul. 2007), arXiv:0706.2344.

[12] Carl Stahle et al., "JWST-RPT-017457: Executive summary: Root cause determination," NASA Document, 1–10(Apr 2011), http://www.jwst.nasa.gov/resources/017457.PDF&link_type=EJOURNAL.

[13] Carl Stahle et al., "JWST-RPT-017774: Executive summary 2d: Define tests to determine whether the existing detectors are qualified for flight," NASA Document, 1–6(Jul 2011), http://www.jwst.nasa.gov/resources/017774.PDF&link_type=EJOURNAL.

[14] James Beletic et al., Proc SPIE in press (2012).

[15] D. Brent Mott, Augustyn Waczynski, Yiting Wen, Bernard J Rauscher, Nicholas Boehm, Meng P Chiao, Lantrinh Degumbia, Greg Delo, Roger Foltz, Emily Kan, David Alexander, Craig Cabelli, Brian Clemons, Joseph Connelly, Alex Dea, Rebecca Derro, Charles Engler, Ali Feizi, Ori Fox, Robert J Hill, Thomas E Johnson, Matthew Lander, Don J Lindler, Markus Loose, Sridhar S Manthripragada, Kevin Novo-Gradac, Wayne D Roher, Robert Rosenberry, Kamdin Shakoorzadeh, Miles T Smith, Donna Wilson, and Joseph Zino, "Characterization of the detector subsystem for the near-infrared spectrograph (nirspec) on the james webb space telescope," High Energy **7021**, 66 (Aug 2008), http://adsabs.harvard.edu/cgi-bin/nph-data_query?bibcode=2008SPIE.7021E.66M&link_type=ABSTRACT.